ACS Photonics

Article

pubs.acs.org/journal/apchd5

Compact Multilayer Film Structures for Ultrabroadband, Omnidirectional, and Efficient Absorption

Chenying Yang,[†,‡,§] Chengang Ji,[‡,§] Weidong Shen,[*,†] Kyu-Tae Lee,[‡] Yueguang Zhang,[†] Xu Liu,[†] and L. Jay Guo[*,‡]

[†]State Key Laboratory of Modern Optical Instrumentation, Department of Optical Engineering, Zhejiang University, Hangzhou, 310027, China

[‡]Department of Electrical Engineering and Computer Science, University of Michigan, Ann Arbor, Michigan 48109, United States

Supporting Information

ABSTRACT: We present a novel scheme for ultrabroadband and omnidirectional perfect absorbers with compact multilayer film structure. Our proposed device shows an average absorption of ~98% over a wide range of wavelengths ranging from 400 to 2000 nm. The ultrabroadband characteristics are achieved with strongly overlapped optical resonances by designing a tandem structure composed of three absorptive materials, while the overall structure features a graded refractive index profile to obtain a wideband antireflection property. In addition to the high efficiency and ultrabroadband absorption, our perfect absorbers exhibit a great angular tolerance up to 60°, which is attributed to not only relatively broad resonances but also negligible propagation phase shifts in ultrathin highly absorbing layers. Lastly, we explore the effect of the number of semiconductor−metal stacks on the performance of the absorber. The presented approach can have tremendous potential for various applications, such as solar−thermal energy harvesting, thermoelectrics, detection, and imaging.

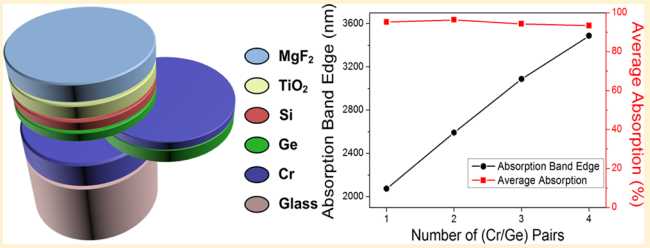

KEYWORDS: *perfect absorber, graded index, ultrabroadband absorption, omnidirectional absorption*

A perfect optical absorber, as a common optical component, is of vital importance in a variety of applications at optical frequencies. In solar−thermal harvesting applications, broadband absorption covering most of the solar spectrum is in critical demand as one of the most important clean energies. For a compact imaging spectrometer based on multichannel filters, the perfect optical absorber is highly desired to prevent the crosstalk between the adjacent channels in the aerospace and semiconductor industries. In recent years, efficient optical absorption in the visible and near-infrared (NIR) region, which can be potentially applied in fields of detecting, imaging, photovoltaics (PVs), and so forth, have attracted enormous interests.[1−29] Among all the designs for the absorbers, broadband absorbers based on metamaterials and transformation optics have been investigated widely and developed in many areas,[10−25] whose absorptions are enhanced by the excitation of the surface plasmon resonance. Especially, the tapered structure consisting of alternating metallic and dielectric thin films is mostly discussed,[19−21] which can be treated as a hyperbolic metamaterial (HMM) waveguide with varying width. Zhou et al. theoretically verified that the broadband absorption of this structure constituted by these closely spaced resonances is formed between the top of the tapered stacks and the cutoff level in the waveguide.[20] As the shadow effect during the evaporation is subtly exploited to construct the tapered structure instead of the complicated process of focused ion beam milling, the time and cost of fabrication are significantly reduced. Liang et al. designed the broadest bandwidth of this structure, which covers a 1−14 μm region.[21] Apart from this tapered structure, Chen et al. proposed a broadband absorber of robust high absorption efficiency for the 900−1600 nm wavelength range by creating patterns of nanoparticles dispersed on a gold film spaced by a thin dielectric layer.[22] Bouchon et al. experimentally demonstrated that a patchwork of four metal−insulator−metal patches leads to an unpolarized wideband omnidirectional absorption constituted by corresponding absorption peaks.[23]

However, all the broadband absorbers described above require either accurate controls or complicated procedures with multiple steps of nanolithography, reactive ion etching, e-beam lithography, or focused ion beam milling, severely limiting their practical applications especially in relatively large areas. Therefore, thin film devices have been pursued as an alternative approach.[26−28] The most common film stack in the previous studies is the dielectric−metal−dielectric (DMD) stack on a reflecting metal.[27,28] The metal layer in the DMD stack is always selected from metals with strong optical absorption, such as chrome, titanium, and nickel, and the thickness of this layer is very thin, allowing multiple reflections within the structure and leading to strong absorption. However, both the

Received: December 2, 2015
Published: March 3, 2016

DOI: 10.1021/acsphotonics.5b00689
ACS Photonics 2016, 3, 590−596

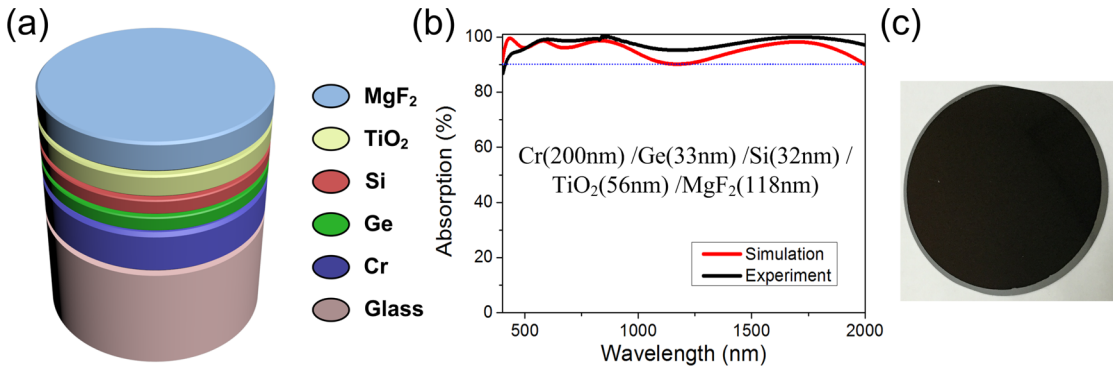

Figure 1. (a) Schematic diagram of the proposed efficient ultrabroadband absorber. (b) Simulated and measured absorption of the proposed absorber targeted for the 400−2000 nm range (film stack 1). (c) Photograph of the fabricated absorber device under normal incidence.

bandwidth and the absorption efficiency are still highly limited for NIR applications. Furthermore, the capability of absorbing a broad spectral range of light with high efficiency from any incident direction regardless of the polarization state of incident light, needed for numerous applications, remains significantly challenging.

Here, we present wafer-scale ultrabroadband absorbers with angular invariance up to 60° in a structure consisting of a stack of various semiconductors on a metallic mirror. Our proposed absorber has a novel device configuration featuring a graded refractive index profile that allows the absorption of the device to be significantly enhanced (~98%) by exploiting antireflection (AR) effects, while the ultrabroadband absorption characteristics are achieved by the designed tandem structure of three absorptive materials with resonances being strongly overlapped. Additionally, the broadband absorption performance with the high efficiency of our absorbers is greatly insensitive with respect to the angle of incidence and the polarization state of incident light, both of which are highly desired properties in diverse applications. We also investigate how the number of semiconductor−metal stacks affects the absorption behavior of the absorber. Furthermore, the proposed device can be fabricated by simple film deposition methods, thereby opening up the possibility of various applications targeting large areas, such as solar−thermal energy harvesting, imaging, and detection.

RESULTS AND DISCUSSION

Figure 1a depicts a schematic diagram of the proposed ultrabroadband and omnidirectional absorber where four thin dielectrics and semiconductors are placed on top of an optically thick metallic substrate. Multiple resonances in each dielectric and semiconductor film at different wavelengths are established, and the overlap of these resonances enables broadband absorption up to 2 μm, which is much longer than the state-of-the-art solar thermal absorber,[27−29] especially than that (400 nm to 1.4 μm) reported in ref 27. It should be noted that the bandwidth can be further widened by inserting more semiconductor−metal stacks, which will be discussed in the later section of this paper. To achieve highly efficient absorption characteristics over a broad range of wavelengths, an absorptive metal with a high refractive index and extinction coefficient is selected as the bottom metal layer. Although chromium (Cr) is chosen for the demonstration in our work, other absorptive metals, such as titanium (Ti), iridium (Ir), tungsten (W), nickel (Ni), or their alloys can also be used (see Figure S1) to attain a similar property. Reflective metals, such as silver (Ag), can also be utilized as the substrate if the absorption needs to be mostly confined within the semiconductor layers, which is required by PV applications (see Figure S2). Considering the absorption $A = 1 - R - T$ with R being the reflectance and T being the transmission, the bottom metallic film is designed to be thick enough (>100 nm) to block any transmitted light so that a perfect absorption property is equal to a zero-reflection property in our system. Four dielectric and semiconductor layers, germanium (Ge), silicon (Si), titanium dioxide (TiO_2), and magnesium fluoride (MgF_2), are subsequently deposited on top of the metallic substrate to create a graded index profiled stack that produce the AR effect,[30] while highly absorbing materials (i.e., Si and Ge) are responsible for the strong absorption at shorter wavelengths. It is important to mention that other dielectric materials with a similar optical constant can be utilized to replace TiO_2 (e.g., by HfO_2 or Ta_2O_5) and MgF_2 (e.g., by SiO_2 or $YLiF_4$), which is given in the Supporting Information (see Figure S3).

For many solar-related applications, such as PV, thermoPV, solar−thermal energy conversion,[31] and solar control glazing windows, achieving high-efficiency broadband absorption characteristics over the full solar spectrum, spanning from ultraviolet (UV) to near-infrared (IR), is highly desired. Targeting at the best absorption behavior over the broad wavelength ranges from 400 to 2000 nm, the required dimension parameters of the device structure are designed by the transfer matrix method. The thickness of each layer is found to be 118, 56, 32, and 33 nm for MgF_2, TiO_2, Si, and Ge layers on the thick Cr metallic substrate. In the device fabrication, the stack was successively deposited by e-beam evaporation with the substrate kept at 150 °C to obtain dense films. Figure 1b shows the calculated and measured absorption spectra of our proposed device at normal incidence, showing great agreement with each other. The average absorption from the simulation and the experiment for wavelengths from 400 to 2000 nm is 95.37% and 97.76%, respectively, both of which show very high absorption efficiency. The slight discrepancy between the measured and calculated results is primarily due to the refractive index values for both Cr and Ge materials, which are sensitive to the preparation condition and quite different from the bulk data in the literature.[32] We should also note that our device design can be modified to apply to areas such as aerospace applications (e.g., to eliminate stray light) and consumer electronics applications of visible−IR detections, all of which require the perfect absorption of wavelengths from 400 to 1200 nm. This can be easily enabled by slightly

DOI: 10.1021/acsphotonics.5b00689
ACS Photonics 2016, 3, 590−596

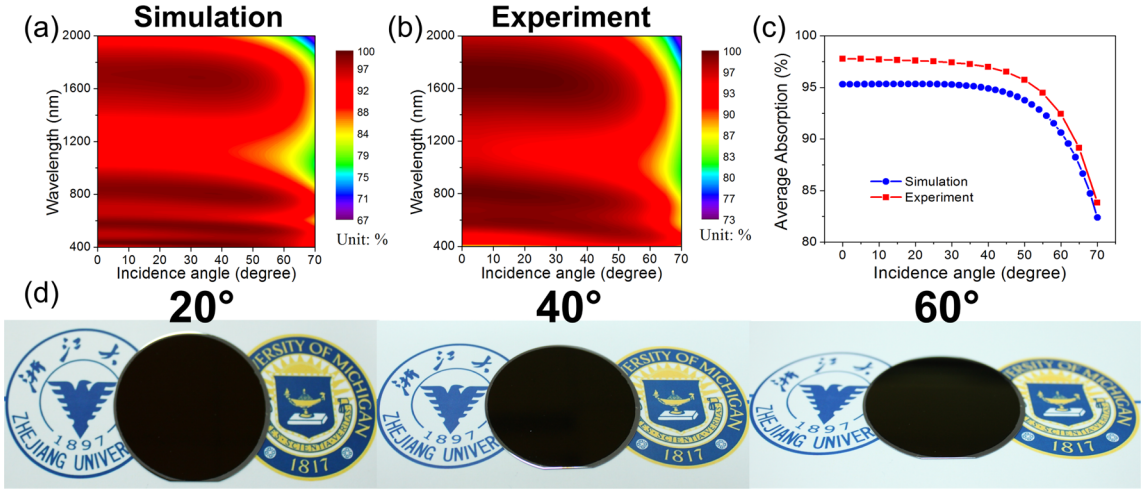

Figure 2. (a) Simulated incident angle resolved spectrum response of the ultrabroadband absorber. (b) Measured incident angle resolved spectrum response of the ultrabroadband absorber. (c) Simulated and measured average absorption of the proposed ultrabroadband absorber for film stack 1 at different incident angles. (d) Optical images of the fabricated absorber taken with indoor ambient light at an oblique incidence of 20°, 40°, and 60°. The diameter of the fabricated device is 2 in.

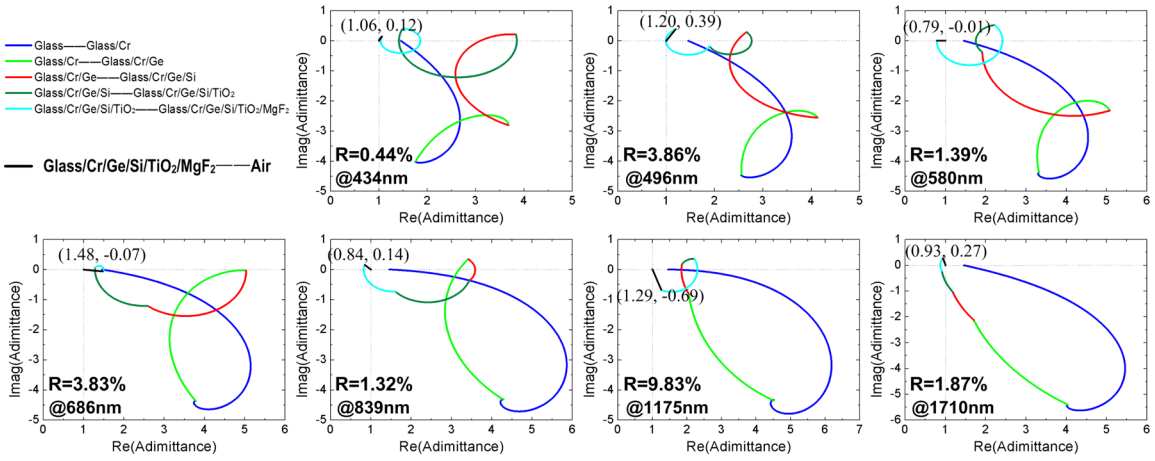

Figure 3. Optical admittance locus of the ultrabroadband absorber for film stack 1 at each peak reflectance wavelength and valley reflectance wavelength. The length of the black line provides a measure of the reflectance of the structure. The reflectance marked in the figure is calculated by the Fresnel reflection formula with the acquired equivalent admittance.

decreasing the thickness of each layer, which moves the resonances toward the shorter wavelength region (see Figure S4). Figure 1c presents a photograph of the fabricated device taken at normal incidence, showing a totally black appearance due to the broadband absorption behavior.

We also explored the angular dependence by both simulation and experiment. The calculated and measured angle-resolved absorption spectra under unpolarized light illumination are displayed in Figure 2a and b, obviously presenting a high angular tolerance feature up to 60° with little variation of the absorption efficiency. To clearly see the effect of the incidence angle beyond 60° on the absorption efficiency of our device, the average absorption efficiency for both the simulation and the experiment is plotted as a function of the incidence angle ranging from 0° to 70°, as shown in Figure 2c. It is clear that the average absorption of our design varies very little up to 40°, while the average absorption efficiency gradually decreases as the incidence angle (greater than 40°) increases further. It is shown that less than a 5% decrease of the average absorption can be kept up to 60°. The optical absorption efficiency is still higher than 80% even at a very large angle (70°). Figure 2d exhibits optical images of the fabricated device taken under indoor ambient light illumination (unpolarized light) at three different angles up to 60°, clearly showing a black color with negligible reflection. Clearly, the absorber shows a robust angular insensitivity property, which is attributed to the broad resonances. In addition, the designed absorber structure consists of two semiconductors with a high refractive index (i.e., Ge and Si), which can lead to a very small angle of refraction into the structure by Snell's law ($n_1 \sin \theta_1 = n_2 \sin \theta/_2$) at IR ranges.[33,34] The strong resonance effects in ultrathin highly absorbing media (i.e., Ge and Si) appearing at visible frequencies,[35] where the phase cancellation effect between the propagation phase shifts through the ultrathin semiconductor films and the reflection phase from the metal film, contribute to the angle-invariant characteristics.[35−37]

We also examine why our absorber structure exhibits highly efficient absorptions. As there is no transmitted light due to the thick metallic substrate, the high absorptions correspond to the low reflections, which can be studied by the optical admittance (inverse of the impedance) at different wavelengths.[30] Figure 3 shows the optical admittance locus of our absorber as the

DOI: 10.1021/acsphotonics.5b00689
ACS Photonics 2016, 3, 590−596

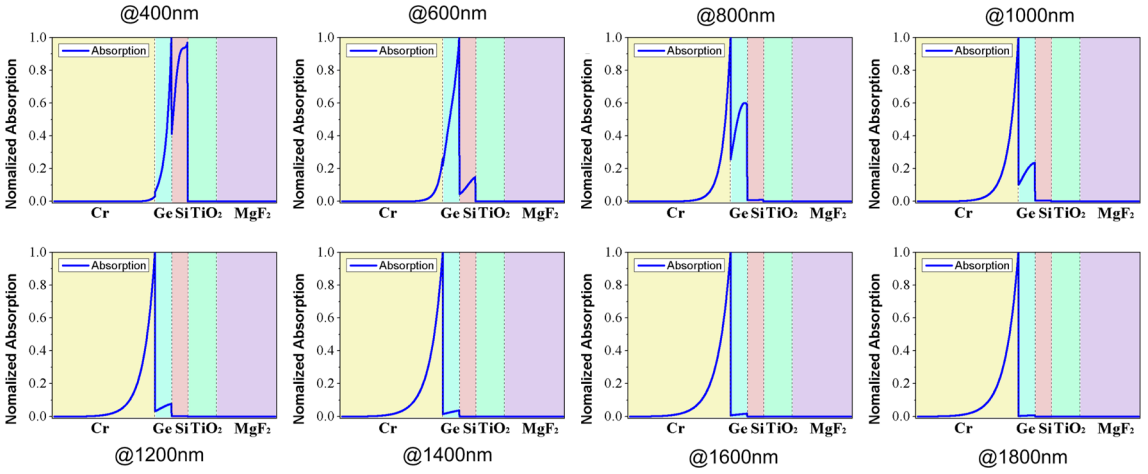

Figure 4. Layer absorption distribution profile of the ultrabroadband absorber for a five-layer structure at different wavelengths, showing the shift of the absorption layer from Si to Cr with increasing wavelength.

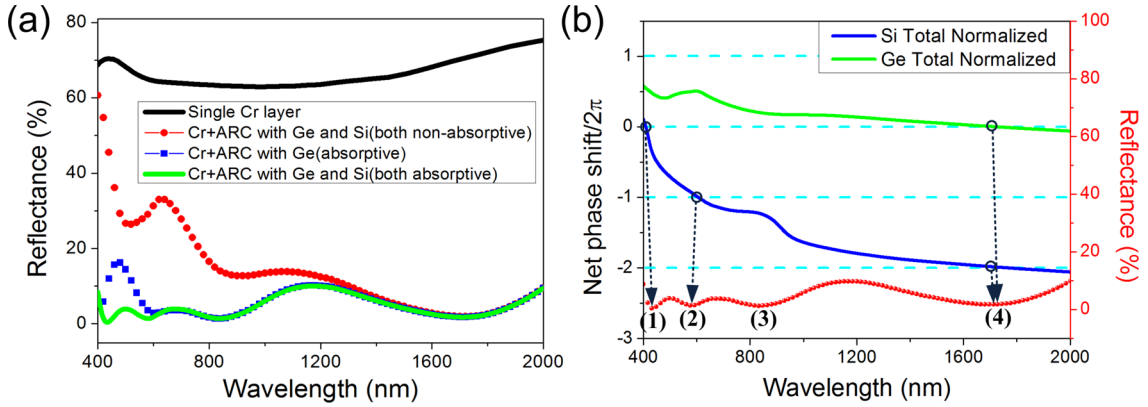

Figure 5. (a) Reflectance of the proposed structure with different materials: practical absorptive materials or nonabsorptive hypothetic materials. ARC: $Ge/Si/TiO_2/MgF_2$ where the extinction coefficients of Ge and Si are set artificially, while the optical constants of TiO_2 and MgF_2 remain invariant, as shown in Figure S5. (b) Net phase shift in each absorptive layer of film stack 1 and the corresponding reflectance curve. The resonances indicated by the phase shift curves (the net phase shifts are equal to a multiple of 2π) are highly consistent with the reflection dips.

thicknesses of the different films increase. At long wavelengths, the $Ge/Si/TiO_2/MgF_2$ combination forms a typical graded index profile of broadband antireflection coatings for the Cr substrate, where the Cr film has the largest refractive index ($n > 4$, $k > 5$) at 839, 1175, and 1710 nm. So, the overall admittance gradually turns small and is finally close to (1, 0), i.e., the index of the incident medium, air. However, the refractive index of Ge is larger than Cr at short wavelengths of 434, 496, 580, and 686 nm. Thus, it is Ge/Cr, rather than the single Cr layer, that has the largest effective admittance, and the admittance of the whole structure is reduced gradually to 1 by $Si/TiO_2/MgF_2$ layers as AR coatings. The graded index profile results in a smaller effective admittance so as to reduce the reflectance of the whole structure gradually. In Figure 3, the length of the black lines (i.e., distance between the termination point and the air) provides a measure of the reflectance of the structure for some wavelengths and is very small for all cases, which is attributed to the graded refractive index profile producing the broadband AR effects. The reflectance of the stack at the corresponding wavelength is calculated by the Fresnel reflection formula and then inserted at the bottom-left corner of each plot in Figure 3.

The ultrabroadband absorption mechanisms are further investigated by studying the main absorptive layers at different wavelengths. A transition of absorption layers from Si to Cr when moving to longer wavelengths is clearly identified. Since the upper TiO_2 layer and MgF_2 layers are lossless in the visible and NIR range, they do not contribute to the absorption but act as the graded index layers for the AR and assist in additional resonances. The absorption takes place in the three lower layers, Si, Ge, and Cr layers, particularly at shorter wavelengths. The absorption distribution profiles of the proposed structure at different wavelengths are shown in Figure 4. Intuitively, as the wavelength increases from the visible to the NIR, the main absorption layers change from Ge/Si layers, to a Ge layer, then to Cr/Ge layers, and eventually to a Cr layer only. This can be easily understood by examining the refractive indices of the layers at various wavelength ranges. From the refractive indices given in Figure S5, we can see that the extinction coefficient of Ge and Si is relatively large from 400 to 500 nm, which makes the Ge and Si layers the main absorption layers within a short wavelength range. As the wavelength increases, the extinction coefficient of Si decreases while that of Ge still remains high, which results in only the Ge layer contributing to the absorption. When the wavelength is longer than 750 nm, the extinction coefficient of Ge decreases while Cr becomes more absorptive with a higher extinction coefficient; thus, the main absorption layers turn to both the Cr layer and the Ge layer.

DOI: 10.1021/acsphotonics.5b00689
ACS Photonics 2016, 3, 590−596

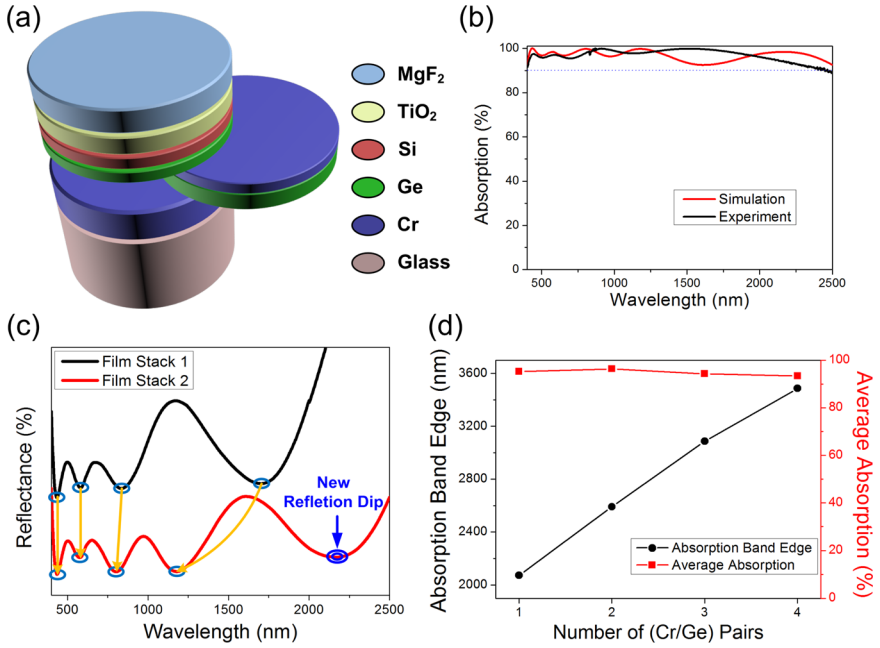

Figure 6. (a) Schematic diagram of the improved ultrabroadband absorber with seven layers by inserting Ge/Cr layers. (b) Simulated and measured absorption of the improved seven-layer absorber. (c) Calculated reflectance spectra of the seven-layer film stack. One addtional reflection dip is created by the inserted Ge/Cr pair as compared to the five-layer structure, as shown with the circled valley reflectance. (d) Relationship between the absorption characteristic and the number of Cr/Ge pairs, indicating that the absorption band can be broadened by 500 nm after inserting every additional Cr/Ge pair.

When the wavelength further goes beyond 1200 nm, Ge becomes transparent; therefore, the absorption occurs only within the Cr layer. On the basis of results in Figure 4 together with those of Figure 3, each of the absorptive materials is responsible for the prefect absorption at specific wavelengths forming the overlapped absorption, whereas the various resonances within corresponding transparent layers on top of those lossy media help to enhance the absorption by increasing the transmission into the absorptive layers with graded indices.

On the basis of the explanations including the antireflection effect in Figure 3 and the tandem absorptive materials aimed for a specific wavelength region in Figure 4, the physical origin of the ultrabroadband absorption of our design is further elaborated here. A simplified film stack composed of the thick chromium layer and the antireflection coatings (ARC) is described in Figure 5a, where the extinction coefficients of Ge and Si are assumed to be zero, while the optical constants of TiO_2 and MgF_2 remain invariant, as shown in Figure S5. By adding the ARC, the reflectance of the device is significantly reduced compared with that of the single thick chromium layer, as shown by the red dotted line. For the wavelengths beyond 1200 nm, the reflection remains the same whether Si and Ge are assumed absorptive or not, which means that the reflection valley at 1710 nm is caused only by the antireflection effects on the absorptive Cr layer. Besides, the reflectance for the 600−900 nm region and the 400−600 nm region can be greatly suppressed when the nonabsorptive hypothetic material is substituted by the actual Ge and Si with absorption, as seen by the blue and green dotted lines, respectively, verifying the tandem absorption property in Figure 4. Moreover, we investigate net phase shifts, involving the propagation phase shift and reflection phase shifts at the top and bottom interfaces, to explore the absorption resonances induced by Ge and Si layers, shown in Figure 5b. As can be seen from the figure, the resonances in each cavity layer, where the net phase shift is equal to a multiple of 2π, correspond to the absorption peaks in Figure 1b. Note that although the ultrathin highly absorbing media are much thinner than the quarter wavelength of incident light ($h \ll \lambda/4n$, where h denotes the thickness of the spacer, λ is the resonant wavelength, and n represents the refractive index of the spacer), the nontrivial phase shift associated with the reflections from the interface between semiconductor (air) and nonideal metals (i.e., finite conductivity) makes up the difference.[35] The positions of the resonances are indicated as the intersection of the dashed and solid lines, all of which correspond exactly to the valley in the reflection spectrum (red scatter line). It is obvious that creating the resonances in different semiconductor materials at different wavelengths (i.e., overlapped resonance behavior) leads to a very strong absorption that corresponds to the reflection dip. For example, the reflection valleys near 434 and 580 nm, which are represented by (1) and (2), respectively, result from the strong resonance absorption of the Si layer. At the long-wavelength region near 1710 nm (4), where all semiconductive and dielectric layers turn transparent, the resonances within the Ge and Si layers indicating the strong absorption of the single Cr substrate are achieved by the enhanced transmission resulting from those resonances within transparent layers, i.e., antireflection effects. Similarly, the reflectance dip at 839 nm (3) resulted from the antireflection effects induced by the Si/TiO_2/MgF_2 stack and the correspondingly enhanced absorption within the Ge layer, which can be seen in Figure 5a. So the resonances of the tandem structure comprising diverse absorptive materials and the antireflection property arising from the graded index profile structure both contribute to the ultrabroadband absorption with high efficiency of this structure.

For the solar-harvesting energy applications, it is highly desired for the solar absorbers to fully cover the solar spectrum up to 2500 nm, which can be accomplished by inserting additional semiconductor−metal stacks. Figure 6a presents a

DOI: 10.1021/acsphotonics.5b00689
ACS Photonics 2016, 3, 590−596

schematic representation of the device, which has an additional cavity (Ge) whose resonance appears at 2200 nm, showing a much improved absorption bandwidth (2.1 μm). The required dimensions of the film stack 2, [Cr(200 nm)/Ge(52 nm)/Cr(21 nm)/Ge(33 nm)/Si(34 nm)/TiO_2(57 nm)/MgF_2(111 nm)], is optimized to achieve the broadest bandwidth with highly efficient absorptions. By placing additional Ge−Cr layers in the five-layer stack, a new resonance is created at longer wavelengths, leading to an even broader bandwidth. The calculated and measured absorption spectra are plotted in Figure 6b, showing the efficient absorption across the entire band of 400−2500 nm with the measured average absorption of 96.82%, which agrees well with the simulated value of 96.71%, implying a great improvement over the state-of-the-art solar thermal absorber,[27−29] especially that in ref 27, showing ∼85% absorption. The efficient absorption bandwidth is dramatically expanded with a new reflection dip appearing, as shown in Figure 6c, which arises from the additional semiconductor−metal stack. Figure 6d shows the calculated absorption bandwidth and the average absorption efficiency as a function of the number of Ge−Cr pairs. We should note that the band edges correspond to the wavelength positions where the absorption efficiency is no lower than 90% and the minimal band edge is kept at 400 nm, which means the results shown in the figure are the maximal band edges. It is clear that increasing the number of Ge−Cr pairs enables the absorption property to be further broadened, while still preserving the high absorption efficiency (>93%). It is thus expected that a much broader absorption characteristic up to 3.5 μm or even more can be achieved by inserting more stacks of semiconductor−metal layers, thereby opening the door to a multitude of new applications.

CONCLUSIONS

In conclusion, a compact multilayer structure for ultrabroadband and omnidirectional perfect absorbers has been demonstrated. The measured average absorption efficiency of our proposed device, which consists of only five layers, is ∼98% for wavelengths from 400 to 2000 nm. The proposed ultrabroadband absorber can present a great angular tolerance up to 60°. It has been demonstrated that the absorption property can be further broadened to 2500 nm, even 3500 nm, or more by inserting pairs of Ge and Cr layers. Both the overlapped resonances of the tandem structure comprising diverse absorptive materials and the antireflection property arising from the graded index profile structure contribute to the ultrabroadband absorption with high efficiency of this structure. The ultrabroadband absorber has great potential in various applications such as on-chip multichannel filters, solar−thermal harvesting, light detecting, and imaging.

METHODS

Simulation. Simulation of the reflectance and absorption of the ultrabroadband absorbers was performed by the transfer matrix method. In our simulation, the wavelength-dependent optical constant of the Cr material was obtained from the data of Palik, and the refractive indices of other materials (Ge, Si, TiO_2, and MgF_2) were experimentally measured by the spectrometry method considering both the reflectance and the transmittance curves, while the refractive index of Ge in visible wavelengths was obtained by the ellipsometry method. The absorption distribution profile of the structure was calculated by commercial electromagnetic field calculation software, FDTD Solutions from Lumerical Inc.

Device Fabrication. The proposed ultrabroadband absorbers were manufactured on the clean substrates of silicon wafers with a diameter of 2 in. The film stacks of five or seven layers were all deposited by e-beam evaporation with a base vacuum pressure better than 2×10^{-3} Pa. During the deposition, the substrates were kept at 150 °C. The deposition rates for Cr, Ge, Si, TiO_2, and MgF_2 are respectively 0.5, 0.2, 0.2, 0.3, and 0.5 nm/s.

Optical Characterization. The reflectance/transmittance measurement at normal incidence was performed by spectrophotometer (Shimadzu UV-3101PC). The angle-resolved reflectance/transmittance was measured by a Cary 7000 angle-resolved spectrometer from Agilent Technologies Inc. The optical constant of germanium in the visible wavelengths was obtained by M-2000 ellipsometry (J.A.Woollam Inc.).

ASSOCIATED CONTENT

Supporting Information

The Supporting Information is available free of charge on the ACS Publications website at DOI: 10.1021/acsphotonics.5b00689.

Additional information (PDF)

AUTHOR INFORMATION

Corresponding Authors

*E-mail (W. Shen): adongszju@hotmail.com. Tel: +86 (571) 87951190. Fax: +86 (571) 87951190.

*E-mail (L. J. Guo): guo@umich.edu. Tel: +1 (734) 6477718. Fax: +1 (734) 7639324.

Author Contributions

§C. Yang and C. Ji contributed equally to this work.

Notes

The authors declare no competing financial interest.

ACKNOWLEDGMENTS

This work was supported by Zhejiang Provincial Natural Science Foundation (No. LY13F050001), National High Technology Research and Development Program 863 (2015AA015904), and National Natural Science Foundation of China (No. 61275161). C.J., K.T.L., and L.J.G. would like to acknowledge the support by the NSF (grants ECCS 1202046 and DMR 1120187).

REFERENCES

(1) Tsakmakidis, K. L.; Boardman, A. D.; Hess, O. 'Trapped rainbow' storage of light in metamaterials. *Nature* **2007**, *450*, 397−401.

(2) Landy, N. I.; Sajuyigbe, S.; Mock, J. J.; Smith, D. R.; Padilla, W. J. Perfect Metamaterial Absorber. *Phys. Rev. Lett.* **2008**, *100*, 207402.

(3) Yang, Z.-P.; Ci, L.; Bur, J. A.; Lin, S.-Y.; Ajayan, P. M. Experimental Observation of an Extremely Dark Material Made By a Low-Density Nanotube Array. *Nano Lett.* **2008**, *8*, 446−451.

(4) Hao, J.; Wang, J.; Liu, X.; Padilla, W. J.; Zhou, L.; Qiu, M. High performance optical absorber based on a plasmonic metamaterial. *Appl. Phys. Lett.* **2010**, *96*, 251104.

(5) Le Perchec, J.; Quémerais, P.; Barbara, A.; López-Ríos, T. Why Metallic Surfaces with Grooves a Few Nanometers Deep and Wide May Strongly Absorb Visible Light. *Phys. Rev. Lett.* **2008**, *100*, 066408.

(6) Wang, J.; Fan, C.; Ding, P.; He, J.; Cheng, Y.; Hu, W.; Cai, G.; Liang, E.; Xue, Q. Tunable broad-band perfect absorber by exciting of

DOI: 10.1021/acsphotonics.5b00689
ACS Photonics 2016, 3, 590−596

multiple plasmon resonances at optical frequency. *Opt. Express* **2012**, *20*, 14871−14878.
(7) Biswas, A.; Eilers, H.; Hidden, F.; Aktas, O. C.; Kiran, C. V. S. Large broadband visible to infrared plasmonic absorption from Ag nanoparticles with a fractal structure embedded in a Teflon AF matrix. *Appl. Phys. Lett.* **2006**, *88*, 013103.
(8) Yang, C.; Shen, W.; Zhang, Y.; Zhao, D.; Liu, X. Multi-narrowband absorber based on subwavelength grating structure. *Opt. Commun.* **2014**, *331*, 310−315.
(9) Zhang, B.; Zhao, Y.; Hao, Q.; Kiraly, B.; Khoo, I.-C.; Chen, S.; Huang, T. J. Polarization-independent dual-band infrared perfect absorber based on a metal-dielectric-metal elliptical nanodisk array. *Opt. Express* **2011**, *19*, 15221−15228.
(10) Aydin, K.; Ferry, V. E.; Briggs, R. M.; Atwater, H. A. Broadband polarization-independent resonant light absorption using ultrathin plasmonic super absorbers. *Nat. Commun.* **2011**, *2*, 517.
(11) Teperik, T. V.; De Abajo, F. G.; Borisov, A.; Abdelsalam, M.; Bartlett, P.; Sugawara, Y.; Baumberg, J. Omnidirectional absorption in nanostructured metal surfaces. *Nat. Photonics* **2008**, *2*, 299−301.
(12) Gan, Q.; Bartoli, F. J.; Kafafi, Z. H. Plasmonic-Enhanced Organic Photovoltaics: Breaking the 10% Efficiency Barrier. *Adv. Mater.* **2013**, *25*, 2385−2396.
(13) Zhu, P.; Jay Guo, L. High performance broadband absorber in the visible band by engineered dispersion and geometry of a metal-dielectric-metal stack. *Appl. Phys. Lett.* **2012**, *101*, 241116.
(14) Cheng, C.-W.; Abbas, M. N.; Chiu, C.-W.; Lai, K.-T.; Shih, M.-H.; Chang, Y.-C. Wide-angle polarization independent infrared broadband absorbers based on metallic multi-sized disk arrays. *Opt. Express* **2012**, *20*, 10376−10381.
(15) Cui, Y.; Xu, J.; Hung Fung, K.; Jin, Y.; Kumar, A.; He, S.; Fang, N. X. A thin film broadband absorber based on multi-sized nanoantennas. *Appl. Phys. Lett.* **2011**, *99*, 253101.
(16) Hendrickson, J.; Guo, J.; Zhang, B.; Buchwald, W.; Soref, R. Wideband perfect light absorber at midwave infrared using multiplexed metal structures. *Opt. Lett.* **2012**, *37*, 371−373.
(17) Sergeant, N. P.; Pincon, O.; Agrawal, M.; Peumans, P. Design of wide-angle solar-selective absorbers using aperiodic metal-dielectric stacks. *Opt. Express* **2009**, *17*, 22800−22812.
(18) Yang, J.; Hu, X.; Li, X.; Liu, Z.; Liang, Z.; Jiang, X.; Zi, J. Broadband absorption enhancement in anisotropic metamaterials by mirror reflections. *Phys. Rev. B: Condens. Matter Mater. Phys.* **2009**, *80*, 125103.
(19) Ji, D.; Song, H.; Zeng, X.; Hu, H.; Liu, K.; Zhang, N.; Gan, Q. Broadband absorption engineering of hyperbolic metafilm patterns. *Sci. Rep.* **2014**, *4*, 4498.
(20) Zhou, J.; Kaplan, A. F.; Chen, L.; Guo, L. J. Experiment and Theory of the Broadband Absorption by a Tapered Hyperbolic Metamaterial Array. *ACS Photonics* **2014**, *1*, 618−624.
(21) Liang, Q.; Wang, T.; Lu, Z.; Sun, Q.; Fu, Y.; Yu, W. Metamaterial-Based Two Dimensional Plasmonic Subwavelength Structures Offer the Broadest Waveband Light Harvesting. Adv. *Adv. Opt. Mater.* **2013**, *1*, 43−49.
(22) Chen, X.; Gong, H.; Dai, S.; Zhao, D.; Yang, Y.; Li, Q.; Qiu, M. Near-infrared broadband absorber with film-coupled multilayer nanorods. *Opt. Lett.* **2013**, *38*, 2247−2249.
(23) Bouchon, P.; Koechlin, C.; Pardo, F.; Haïdar, R.; Pelouard, J.-L. Wideband omnidirectional infrared absorber with a patchwork of plasmonic nanoantennas. *Opt. Lett.* **2012**, *37*, 1038−1040.
(24) Aubry, A.; Lei, D. Y.; Maier, S. A.; Pendry, J. B. Broadband plasmonic device concentrating the energy at the nanoscale: The crescent-shaped cylinder. *Phys. Rev. B: Condens. Matter Mater. Phys.* **2010**, *82*, 125430.
(25) Lei, D. Y.; Aubry, A.; Maier, S. A.; Pendry, J. B. Broadband nano-focusing of light using kissing nanowires. *New J. Phys.* **2010**, *12*, 093030.
(26) Du, G.-Q.; Zhang, L.-W.; Jiang, H.-T. Broadband and omnidirectional absorption in heterostructures with a highly absorptive metallic film and a dielectric Bragg reflector. *J. Appl. Phys.* **2011**, *109*, 063525.
(27) Deng, H.; Li, Z.; Stan, L.; Rosenmann, D.; Czaplewski, D.; Gao, J.; Yang, X. Broadband perfect absorber based on one ultrathin layer of refractory metal. *Opt. Lett.* **2015**, *40*, 2592−2595.
(28) Li, X.-F.; Chen, Y.-R.; Miao, J.; Zhou, P.; Zheng, Y.-X.; Chen, L.-Y.; Lee, Y.-P. High solar absorption of a multilayered thin film structure. *Opt. Express* **2007**, *15*, 1907−1912.
(29) Li, P.; Liu, B.; Ni, Y.; Liew, K. K.; Sze, J.; Chen, S.; Shen, S. Large-Scale Nanophotonic Solar Selective Absorbers for High-Efficiency Solar Thermal Energy Conversion. *Adv. Mater.* **2015**, *27*, 4585−4591.
(30) Macleod, H. A. *Thin Film Optical Filters*; CRC: Boca Raton, 2010.
(31) http://www.solar-thermal.com/.
(32) Palik, E. D. *Handbook of Optical Constants of Solids*; Academic: New York, 1985.
(33) Lee, K.-T.; Ji, C.; Banerjee, D.; Guo, L. J. Laser Photon. *Rev.* **2015**, *9*, 354−362.
(34) Yang, C.; Shen, W.; Zhang, Y.; Li, K.; Fang, X.; Zhang, X.; Liu, X. Compact multilayer film structure for angle insensitive color filtering. *Sci. Rep.* **2014**, *5*, 9285.
(35) Kats, M. A.; Blanchard, R.; Genevet, P.; Capasso, F. Nanometre optical coatings based on strong interference effects in highly absorbing media. *Nat. Mater.* **2013**, *12*, 20.
(36) Lee, K.-T.; Seo, S.; Lee, J. Y.; Guo, L. J. Strong resonance effect in a lossy medium-based optical cavity for angle robust spectrum filters. *Adv. Mater.* **2014**, *26*, 6324−6328.
(37) Lee, K.-T.; Lee, J. Y.; Seo, S.; Guo, L. J. Colored ultrathin hybrid photovoltaics with high quantum efficiency. *Light: Sci. Appl.* **2014**, *3*, e215.

DOI: 10.1021/acsphotonics.5b00689
ACS Photonics 2016, 3, 590−596